JOURNAL OF GEOPHYSICAL RESEARCH, VOL. 112, D15112, doi:10.1029/2006JD007973, 2007

Three-dimensional SF_6 data and tropospheric transport simulations: Signals, modeling accuracy, and implications for inverse modeling

M. Gloor,[1] E. Dlugokencky,[2] C. Brenninkmeijer,[3] L. Horowitz,[4] D. F. Hurst,[2,5] G. Dutton,[2,5] C. Crevoisier,[6] T. Machida,[7] and P. Tans[2]

Received 26 August 2006; revised 5 December 2006; accepted 18 April 2007; published 15 August 2007.

[1] Surface emissions of SF_6 are closely tied to human activity and thus fairly well known. They therefore can and have been used to evaluate tropospheric transport predicted by models. A range of new atmospheric SF_6 data permit us to expand on earlier studies. The purpose of this first of two papers is to characterize known and new transport constraints provided by the data and to use them to quantify predictive skill of the MOZART-2 atmospheric chemistry and transport model. Main noteworthy observational constraints are (1) a well-known steep N-S gradient at the surface confined to an $\approx 40^\circ$ wide latitude band in the tropics; (2) a fairly uniform N-S gradient in the upper troposphere; (3) an increase in the temporal variation in upper troposphere Northern Hemisphere records with increasing latitude; (4) a negative SF_6 gradient in Northern Hemisphere vertical profiles from the surface to 8 km height, but a positive gradient in the Southern Hemisphere; and (5) a clear reflection in surface records of large-scale seasonal atmosphere movements like the undulations of the Intertropical Convergence Zone (ITCZ). Comparison of observations with simulations reveal excellent modeling skills with regards to (1) large-scale annual mean latitudinal gradients at remote surface sites (relative bias of N-S hemisphere difference $\leq$ 5%) and aloft ($\approx$10 km, relative bias $\leq$ 25%); (2) seasonality in signals at remote sites caused by large-scale movements of the atmosphere; (3) time variation in upper troposphere records; (4) ''faithfulness'' of advective transport on timescales up to $\approx$1 week; and (5) the general shapes and seasonal variation of vertical profiles. The model (1) underestimates the variation in the vertical of profiles, particularly those from locations close to high emissions regions, and (2) overestimates the difference in SF_6 between the planetary boundary layer (PBL) and free troposphere over North America, and thus likely Eurasia, during winter by approximately a factor of 2 (STD $\approx$ 100%). The comparisons permit estimating lower bounds on representation errors which are large for sites close to continental outflow regions. Given the magnitude of the signals and signal variance, SF_6 provides a strong constraint on interhemispheric transport, PBL ventilation, dispersion pathways of northern midlatitude surface emissions through the upper troposphere, and large-scale movements of the atmosphere.

Citation: Gloor, M., E. Dlugokencky, C. Brenninkmeijer, L. Horowitz, D. F. Hurst, G. Dutton, C. Crevoisier, T. Machida, and P. Tans (2007), Three-dimensional SF_6 data and tropospheric transport simulations: Signals, modeling accuracy, and implications for inverse modeling, *J. Geophys. Res.*, *112*, D15112, doi:10.1029/2006JD007973.

[1]Earth and Biosphere Institute and School of Geography, University of Leeds, Leeds, UK.
[2]Global Monitoring Division, Earth System Research Laboratory, NOAA, Boulder, Colorado, USA.
[3]Max-Planck Institute for Chemistry, Mainz, Germany.
[4]Geophysical Fluid Dynamics Laboratory, NOAA, Princeton, New Jersey, USA.
[5]Also at Cooperative Institute for Research in Environmental Sciences, University of Colorado, Boulder, Colorado, USA.
[6]Atmospheric and Oceanic Sciences Program, Princeton University, Princeton, New Jersey, USA.
[7]National Institute for Environmental Studies, Tsukuba, Japan.

0148-0227/07/2006JD007973$09.00

1. Introduction

[2] Atmospheric pollutant transport and dispersion can be predicted in principle with atmospheric transport models which solve the tracer transport equation numerically given wind fields and vertical air mass fluxes associated with convection. The transport fields are derived by blending regularly recorded observations characterizing the state of the atmosphere and the principles of fluid dynamics using data assimilation mathematics [e.g., *Simmons and Gibson*, 2000]. Maximal resolution of available fields at NCEP is

currently $1/3^\circ \times 1/3^\circ$ longitude by latitude, with 64 layers in the vertical and 3 hour time resolution.

[3] There is a range of applications of transport models for which the accuracy of the model predictions needs to be known but often is not properly taken into account, partially because accuracy has not been assessed quantitatively. Such applications include prediction of pollution episodes and related air quality, as well as inferential approaches to estimate surface fluxes of greenhouse gases like CO_2. Thereby atmospheric transport is ''inverted'' to estimate fluxes from observed atmospheric patterns. Proper inclusion of model transport uncertainties is critical for this application [e.g., *Gloor et al.*, 2000].

[4] A powerful means to assess the accuracy of predicted tracer transport and dispersion (biases and uncertainties (standard deviation of model data differences)), and to learn about transport itself, is by analysis of observed and modeled dispersion of trace substances with known surface fluxes and with no volume sources and sinks (i.e., no in situ production or loss in the atmosphere). A trace substance that comes close to these requirements is SF_6. Surface fluxes of SF_6 include anthropogenic emissions from applications in industry and very minor uptake by the oceans. SF_6 is inert throughout the troposphere and stratosphere and is slowly photolyzed in the mesosphere, resulting in an estimated atmospheric lifetime of $\approx$3200 years [*Ravishankara et al.*, 1993]. Furthermore the solubility of SF_6 is small thus the uptake rate by the oceans is very slow, making the oceanic and mesosphere sinks negligible compared to anthropogenic emissions. Therefore, on timescales relevant to tropospheric transport, up to a few years, SF_6 can be considered to be conserved in the atmosphere (i.e., to have no sources and sinks) and to be only changed by anthropogenic emissions at the Earth's surface.

[5] Industrial applications of SF_6 are related to its special physical properties which result from its extremely strong atomic bonds. SF_6 is resistant to disintegration into a plasma up to very high voltage and is chemically highly inert. Accordingly it is used in industry as insulating material in high voltage switch gear and as a ''blanket material'' (protecting layer) in processes involving molten reactive metals, like die casting and magnesium production. The close ties to human ''activity'' permit SF_6 emissions to be estimated roughly by distributing national sales numbers spatially within each nation according to electrical energy use. This is in essence the procedure followed by *Olivier* [2002] on whose emission maps we base our simulations, with some modifications that circumvent the uncertainty in these maps caused by the lag between SF_6 acquisition and release to the atmosphere. Quantitative uncertainty estimates of the *Olivier* [2002] emissions maps are unfortunately not available, nonetheless *Olivier* [2002, p. 1] state ''the uncertainty in the resulting data set at national level may be substantial... and even more so for the F-gases.''

[6] Previously, SF_6 observations were used in several studies to estimate transport characteristics of the troposphere and to evaluate accuracy (biases and uncertainties) of transport models [*Ko et al.*, 1993; *Maiss and Levin*, 1994; *Maiss et al.*, 1996; *Geller et al.*, 1997; *Denning et al.*, 1999; *Kjellstrom et al.*, 2000; *Peters et al.*, 2004]. In recent years a range of new atmospheric SF_6 measurements have become available which permit a more complete assessment of the accuracy of transport prediction and understanding of tropospheric transport. New data include upper air ($\sim$10 km) aircraft based transects, Siberian vertical profiles, and a quasi-continuous record from the North American tall tower station in northern Wisconsin, USA, which is remote from large metropolitan areas.

[7] The paper serves two purposes. First we want to identify and quantify transport constraints contained in the current atmospheric SF_6 data set. We then use these constraints to determine the accuracy of transport predicted by the MOZART-2 model of *Horowitz et al.* [2003]. So far, predictive nonreactive tracer transport skills of the MOZART-2 model have not been assessed, even though the model is widely used in the atmospheric chemistry community. In a companion paper, we use the data constraints together with the simulations to learn more about tropospheric transport.

[8] This paper is structured as follows. First we specify available data, their relation to surface emissions, and specifics of the model and modeling setup. We then analyze in parallel constraints provided by the different SF_6 data on tropospheric transport and accuracy of transport modeling. Finally we summarize signal, signal variance, and modeling accuracy across the spectrum of transport processes that atmospheric SF_6 is sensitive to and discuss some implications.

2. Data, Model, and Simulation Setup

2.1. Data and Transport Processes

[9] Locations of the sampling sites for which SF_6 data are available for this study are shown in Figure 1 superposed on the spatial distribution of SF_6 emissions for 1995 estimated by *Olivier* [2002]. The data include weekly surface records based on flask sampling from the National Oceanic and Atmospheric Administration, Earth System Research Laboratory (NOAA ESRL, USA) since March 1997, monthly vertical aircraft profiles based on flask sampling from NOAA ESRL and NIES (Japan) since January 1999, quasi-continuous, in situ measurements by NOAA ESRL gas chromatographs (GCs) at one tall tower site (1996–2000) and four surface observatories since 2001, and upper troposphere transects based on flask sampling in passenger aircraft leaving from and returning to Germany (Max-Planck Institute for Chemistry, Mainz, Germany) since January 1999. Precision of flask sample analysis at NOAA ESRL is 0.04 ppt (1σ). For comparison the global surface mean mixing ratio was 5.4 ppt in 2003 and was increasing by 0.2 ppt yr^{-1}. Other labs report a similar precision. Though there has not been a ''formal'' intercomparison of SF_6 standards between these three laboratories, a $\sim$3 ppt NOAA ESRL standard was assayed by the University of Heidelberg in 1996, and results from these two labs were in good agreement [*Geller et al.*, 1997]. The accuracy of measurements is indeterminable because errors (if any) in the absolute calibration scale cannot be quantitatively assessed. The data allow us to constrain a range of atmospheric transport processes which are summarized in Table 1.

2.2. Model

[10] The MOZART model version we use is documented in detail by *Horowitz et al.* [2003], thus we summarize it

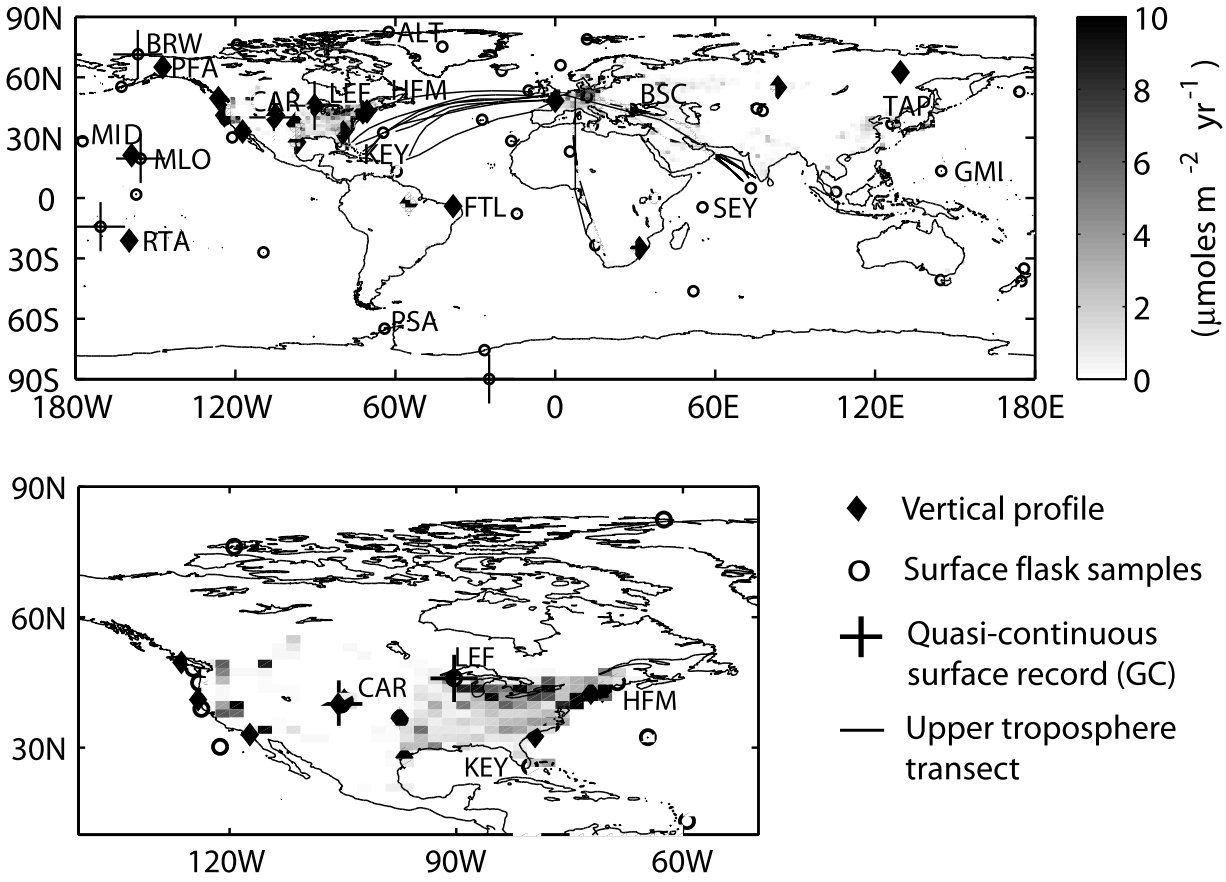

Figure 1. Surface emissions for 1995 estimated by *Olivier* [2002] on the basis of sales and electrical energy use data. Symbols indicate locations where atmospheric SF_6 concentrations are measured.

only briefly. The MOZART-2 model solves the tracer transport equation on a regular grid with a hybrid sigma-pressure coordinate in the vertical using the *Lin and Rood* [1996] scheme complemented with a pressure fixer described by *Horowitz et al.* [2003]. The grid cell dimensions can be chosen at will. Meteorological fields from a variety of sources can be used. For the simulations shown here meteorological fields are from National Centers for Environmental Prediction (NCEP) with a spatial resolution of approximately 1.875° × 1.875° longitude by latitude (T62 resolution), 28 layers in the vertical and time resolution of 6 hours. In addition to horizontal winds and surface pressure, which are used directly to predict tracer transport and dispersion, specific humidity and surface fluxes of heat

Table 1. SF_6 Data and Transport Processes They Reflect

Data	Diagnostic	Process Diagnosed
Surface flask samples	latitudinal differences	interhemispheric transport, interhemispheric difference per flux strength
	zonal differences	zonal transport
	seasonality	seasonal large-scale atmosphere variations (e.g., ITCZ movement, Arctic winter circulation)
Surface quasi-continuous records	timing "pollution" events	faithfulness of advective transport on continental to hemispheric spatial scales
Tall tower quasi-continuous record	timing "pollution" events	faithfulness of advective transport
	magnitude of pollution events	PBL-free troposphere exchange
Vertical aircraft profile (flasks)	PBL-free troposphere difference	PBL signal per flux strength, PBL ventilation rate
	zonal variation in PBL free troposphere difference	PBL ventilation rate
	pollution events	dispersion mode and pathway in lower troposphere
	relation between upper and lower troposphere latitudinal gradients and "events"	transport pathways through upper troposphere
Upper troposphere transects (flasks)	latitudinal gradients	interhemispheric transport
	time variation in relation to lower troposphere	transport pathways through upper troposphere

and momentum are used to derive transport fields related to dissipative processes operating at scales smaller than the transport model grid. Three subgrid-scale processes are represented by MOZART-2: vertical diffusion in the planetary boundary layer, characterized by both mechanically driven turbulence and turbulence related to dry convection, is represented by the *Holtslag and Boville* [1993] scheme, shallow and midlevel convection by the *Hack* [1994] scheme and deep convection by the *Zhang and McFarlane* [1995] scheme. For the simulations shown here the meteorology fields have been regridded to a regular grid with exactly 1.875° × 1.875° longitude by latitude resolution, using the spectral (spherical harmonics) routine SPHEREPACK. The lowermost 1 km of the model grid includes 5 layers. The simulation time step is 15 minutes and time resolution of archived output fields is 3 hours. Simulations are started in January 1995 from an atmosphere with no SF_6. The simulated mixing ratio distribution reaches a stationary state characterized by nearly time-independent spatial differences after approximately 3 years.

[11] For the observation-simulation comparisons, the model is sampled at the correct time and an estimate of the observed atmospheric mean SF_6 at 1 January 1995 of 3.28 ppt is added to the simulations to permit comparison with the data (as the simulations start on 1 January 1995 from an SF_6 free atmosphere). As data are sparse before 1995 we have estimated the atmospheric mean SF_6 from the Neumayer site record [*Maiss et al.*, 1996], the only available observational record from the Southern Hemisphere high latitudes before 1995, to which we add half of the observed mean N-S gradient from the years 1998 to 2000. Estimating the mean atmospheric interhemispheric difference from 1998–2000 data is justified because emissions during 1995 to 2000 have stayed fairly constant (as is evident from growth rate inferred from the atmospheric records). We estimate the uncertainty of the 1 January 1995 atmospheric mean as ±0.04 ppt.

2.3. SF_6 Surface Emissions

[12] For use in the simulations, we scaled SF_6 surface emission maps of *Olivier* [2002] with the mean tropospheric SF_6 record in order that emissions are consistent with the time course of the atmospheric burden. Surface emission maps were available for 1970, 1980, 1990, and 1995. Atmospheric records for scaling of the emission patterns were taken from the Cape Grim, Tasmania (40.66°S, 144.66°E) record for the period from 1978 to 1994, measured by *Maiss and Levin* [1994], and the global composite from NOAA ESRL for the period from 1995 to 2004 (Dlugokencky et al., in prep.). As the time derivative of a time series amplifies high frequencies that are due to sampling and local transport variation rather than variation in surface fluxes, we low-pass filtered the Cape Grim and NOAA ESRL global composite atmospheric records. We used a second-order Butterworth filter whose cutoff frequency was chosen such that variations on timescales smaller than 20 months were removed. For the period before 1978 a linear growth rate was assumed with slope adjusted such that the implied atmospheric SF_6 burden for September 2003 matched the observed inventory (dry mass of the atmosphere used: $5.15 * 10^{21}$ g). Spatial patterns were interpolated linearly in time within each five year period. Because spatial surface emission maps were not available after 1995, we expect model-data disagreement of large-scale spatial differences to increase with time after 1995 because of spatial shifts in emissions.

3. Data Transport Constraints and Model Accuracy Assessment

3.1. Near-Surface Signals

3.1.1. Interhemispheric Difference

[13] The most used constraint in the literature provided by SF_6 is the interhemispheric difference, defined here as the annual mean difference between the 20–90°N and 20–90°S means. It is the result, and thus a diagnostic, of the combined effects of all processes that contribute to interhemispheric transport.

[14] The observed latitudinal distribution of surface observations at remote locations in Figure 2 reveals two main noteworthy features. First there are large differences over short distances in a small latitude band between 30°N and 50°N. The variations show up in two dimensions, both longitude and latitude. Comparison with the structure of surface emissions (Figure 2, bottom) shows that these signatures mirror the localized nature of the emissions. Secondly, there is a strong N-S decrease confined to a fairly narrow band between 10°S and 25°N. Outside the 10°S and 50°N band, surface SF_6 is nearly uniform with latitude in each hemisphere.

[15] Comparison of observed and simulated annual mean N-S differences at remote surface sites (Figure 2) reveal excellent agreement between simulations and data (quantified in Table 2). Relative differences between predicted and observed interhemispheric difference over the time course of a year are 5%. The correlation coefficient of model result versus observations as a function of latitude is 0.99, thus spatial variation over a few degrees is very well captured by the model as well. The RMS error over the time course of a year of observation model prediction differences relative to the N-S signal is ≈8%. The simulation data differences arise both because of uncertainties in the spatial distributions of the fluxes and imperfections in the modeling. They are thus an upper bound to modeling bias and uncertainty.

[16] Standard deviation over the course of a year of data-model deviation of the interhemispheric difference is remarkably small (Table 2). Therefore signal to "noise" of the data constraint provided by interhemispheric differences is ≈10 which means the diagnostic is indeed a strong constraint on model performance. Knowledge of the total flux permits us to determine the expected surface N-S difference signal per flux for emissions located primarily within 30°N to 60°N: $\delta(X_N - X_S)/\delta F \approx 0.36\ ppt\ SF_6/(5.24\ ktSF_6\ yr^{-1}) = 0.32\ ppt/(mol\ s^{-1})$. A similar N-S gradient to flux sensitivity is expected for atmospheric CO_2 due to fossil fuel emissions, because fossil fuel emissions are tied similarly to human "activity" (the relation for CO_2 is obtained by multiplication with the ratio of the molar masses of SF_6 and C respectively which results in $\delta\ (X_N - X_S)/\delta F \approx 0.83\ ppm\ (PgC\ yr^{-1})^{-1}$). The relation permits us also to roughly propagate uncertainties in modeling to uncertainties in the N-S contrast of fluxes.

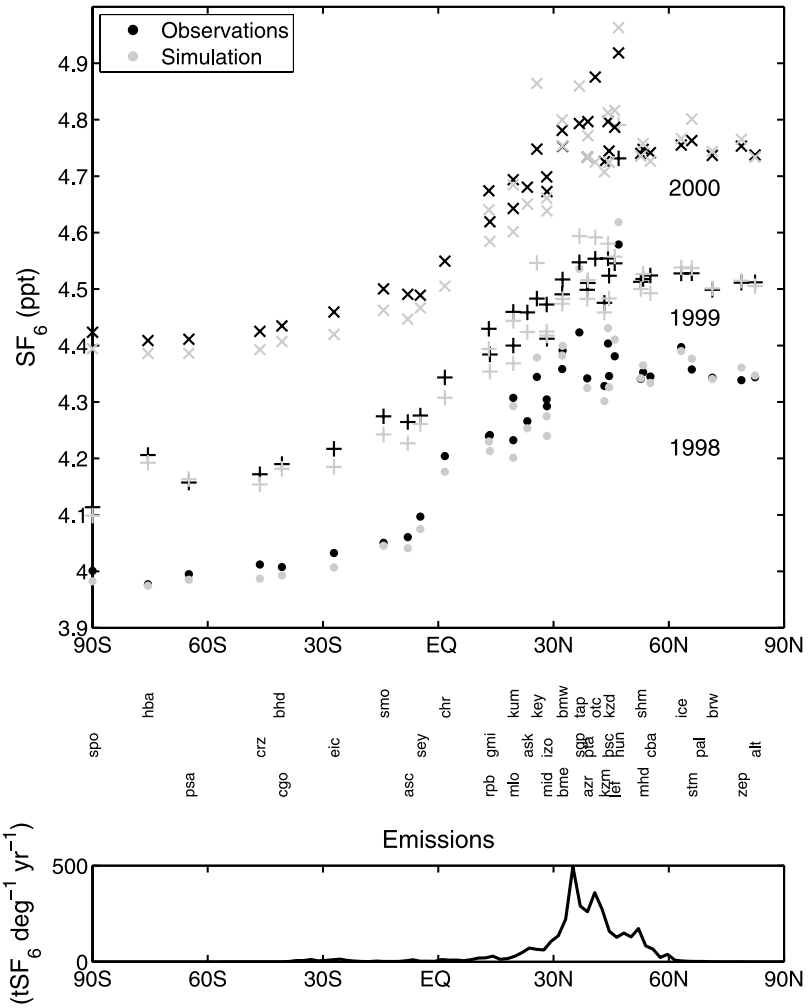

Figure 2. (top) Comparison of observed (dark) and simulated (light) latitudinal distribution of annual mean surface data from NOAA ESRL and (bottom) zonally integrated emissions for 1995 (i.e., the meridional integral of the displayed emissions $\int_{\pi/2}^{\pi/2} f(\theta)\, d\theta \approx 6000\ kt\ yr^{-1}$ equals the total annual emissions).

Table 2. Summary of Model Predictive Skills of the Latitudinal Mean Distribution and Interhemispheric Difference (Difference Between 20–90°N Mean and 20–90°S Mean) at Remote Surface Sites[a]

	Observed Signal		Simulated Signal	
Year	$\lvert\Delta X^{obs}_{N-S}\rvert$, ppt	$Std(\Delta\ X^{obs}_{N-S})$, ppt	$\lvert\Delta X^{sim}_{N-S}\rvert$, ppt	$Std(\Delta\ X^{sim}_{N-S})$, ppt
1998	0.36	0.05	0.38	0.03
1999	0.34	0.06	0.36	0.05
2000	0.33	0.03	0.36	0.03

	Data-Model Differences			
Year	$\frac{\lvert\Delta X^{obs}_{N-S}-\Delta X^{sim}_{N-S}\rvert}{\lvert\Delta X^{obs}_{N-S}\rvert}$ (× 100%)	$\frac{RMS}{\lvert\Delta X^{obs}_{N-S}\rvert}$ (× 100%)	$Std(\Delta\ X^{obs}_{N-S} - \Delta\ X^{sim}_{N-S})$, ppt	Latitude Correlation r
1998	6.5%	8%	0.02	0.99
1999	4%	8%	0.02	0.99
2000	9%	13%	0.03	0.97

[a]X is dry-air mole fraction. Standard deviations (Std) are calculated with respect to time in the year on the basis of 12 monthly samples per year, RMS is calculated as RMS = $\sqrt{1/N\sum_{i=1}^{N}\left(X_i^{\mathrm{obs}} - X_i^{\mathrm{sim}}\right)^2}$ where N is the number of surface stations and X_i are annual means, and the correlation with respect to latitude is calculated on the basis of annual mean mixing ratios.

3.1.2. Variation on Seasonal Timescales

[17] The seasonal variation at remote surface sites holds clues about tropospheric transport related to large-scale movements of the troposphere like the seasonal north-south oscillation of the ITCZ. It furthermore provides an estimate of the so-called representation error. ''Representation error'' refers to model-data differences due to mismatch in scale between ''point'' measurements and surface flux and model grid resolution. To elucidate information on large-scale atmospheric movements, we focus on 7 remote sites (Palmer Station, Antarctica (PSA), 64.92°S, 64.00°W, Ascension Island (ASC), 7.92°S, 14.42°W, Seychelles (SEY), 4.67°S, 55.17°N, Guam (GMI), 13.43°N, 144.78°E, Mauna Loa (MLO), 19.53°N, 155.58°W, Midway (MID), 28.22°N, 177.37°W, Barrow (BRW), 71.32°N, 156.6°W and Alert (ALT), 82.45°N, 62.52°W, and for representation errors on further 4 sites located either on continents or in continental outflow regions (Key Biscayne (KEY) 25.67°N, 80.2°W, Taeahn Peninsula (TAP), 36.73°N, 126.13°E, Black Sea, Constanta, Romania (BSC), 44.17°N, 28.68°E, and Wisconsin (LEF), 45.93°N, 90.27°W).

[18] The further to the south a site is located, the weaker the seasonal cycle, as illustrated by the PSA (64.92°S, 64.00°W)record in Figure 3 (at South Pole (SPO), the variation is smaller still). On the basis of this observation we use the PSA record as a reference for analyzing records from sites located to the north of PSA. We do this by subtracting a linear trend estimated from the record at Palmer Station, Antarctica (PSA) (topmost plot) from each site's record. As we are only interested in the seasonal cycle relative to a constant growth rate (here estimated from PSA) we also subtracted separately from each site's record its annual mean (Figure 3). We refer to differences between a sites record and the PSA record as anomalies.

[19] At sites close to the equator like SEY (4.67°S, 55.17°N) or Christmas Island (CHR), 1.7°N, 157.17°W, the observations flip seasonally between positive anomalies during winter and negative anomalies during summer. The seasonal switch is related to the N-S undulation of the ITCZ which follows the seasonal variation of maximum solar influx on the Earth (Figure 4). Thus depending on the relative location of the site to the ITCZ, the site samples either Northern or Southern Hemisphere air. Consistent with this interpretation, there is indeed a one to one relation between precipitation seasonality at SEY (4.67°S, 55.17°N) and SF_6 (not shown).

[20] A similar but likely unrelated signature is seen in the MID (28.22°N, 177.37°W) and GMI (13.43°N, 144.78°E) records: positive anomalies during the first half of the year followed by negative anomalies during the second half of the year. The observed pattern could be due to the different regions sampled during winter compared to summer, as reflected by mean wind patterns in relation to the site locations (Figure 4). As a consequence of summer surface low and winter high surface pressure over Eurasia, the sites sample northern Eurasian continental air during winter while during summer they sample air from North America. Another explanation could be enhanced flushing of the continental PBL by convection during summer. Enhanced flushing during summer adds more ''low'' SF_6 air from the free troposphere to the PBL over the Northern Hemisphere continents, thereby reducing the abundance of SF_6 in the PBL. Continental air advected to GMI and MID from the continents would therefore tend to be lower in SF_6 during summer compared to winter. Some support for this explanation comes from the Wisconsin tower (LEF) site which shows a fairly similar time course as GMI and MID.

[21] The ''high-latitude'' stations BRW (71.32°N, 156.6°W) and ALT (82.45°N, 62.52°W) show qualitatively yet another behavior. During the period from March to July the growth rate is similar to the PSA reference record, followed by a decrease in the growth rate resulting in negative anomalies during autumn, and an increase in the growth rate during October to February resulting in positive anomalies during winter. This ''recovery'' phase may possibly be a reflection of the very strong atmospheric stability and associated circulation during winter over the Northern Hemisphere continents [e.g., *Lloyd et al.*, 2002; J. Lloyd, unpublished Siberian meteorology and atmospheric CO data related to human activity, 1998]. Related to the strong air column stability is the Arctic Haze phenomenon lasting from December to March, which coincides roughly with the ''recovery'' period at BRW and ALT.

[22] Finally there is a contrast in monthly and interannual signal variation at remote, oceanic sites compared to sites located in coastal outflow regions like Key Biscayne (KEY, 25.67°N, 80.2°W) and Taeahn Peninsula (TAP, 36.73°N, 126.13°E) (Figure 3). There the data exhibit considerably more variability.

[23] The transport constraints provided by biweekly/monthly data are thus (1) the seasonality at tropical sites caused by ITCZ movement, (2) the seasonality at Northern Hemisphere midlatitude sites caused by intensified convective PBL ventilation during summer, (3) the winter SF_6 increase at northern high latitudes caused possibly by pollution trapping during winter (Arctic haze) and (4) an estimate of the representation error for SF_6.

[24] At remote sites with a seasonal signal the model captures signatures well both with regards to phase and amplitude (correlation coefficients ~0.8, Table 3) indicating that the model reproduces the effect of seasonal large-scale atmospheric movements well. There is a larger discrepancy between data and model at continental outflow sites and to lesser extent continental sites. Using the standard deviation over the year as an estimate of representation error for SF_6 we find up to 10 fold larger values at ''continental outflow'' sites like TAP (36.73°N, 126.13°E) and KEY (25.67°N, 80.2°W) and continental sites like LEF (45.93°N, 90.27°W) compared to background sites like MLO (19.53°N, 155.58°W). Because fossil fuel CO_2 and SF_6 emissions are both emitted by energy-related human activities, subgrid-scale spatial patterns are likely very similar. As atmospheric CO_2 is also influenced by land biosphere-atmosphere exchange fluxes, the data-model mismatch or model ''representation error'' estimated from SF_6 may be scaled with the ratio of fossil fuel to SF_6 emissions to obtain an estimate of the lower bound of this quantity for CO_2 which is ≈2.5 ppm at TAP (36.73°N, 126.13°E) and KEY (25.67°N, 80.2°W) (the ratio between CO_2 fossil fuel emissions and SF_6 emissions for 2000 is $\approx 2.7*10^5$ gCO_2/gSF_6 ≈12.16 ppm CO_2/ppt SF_6).

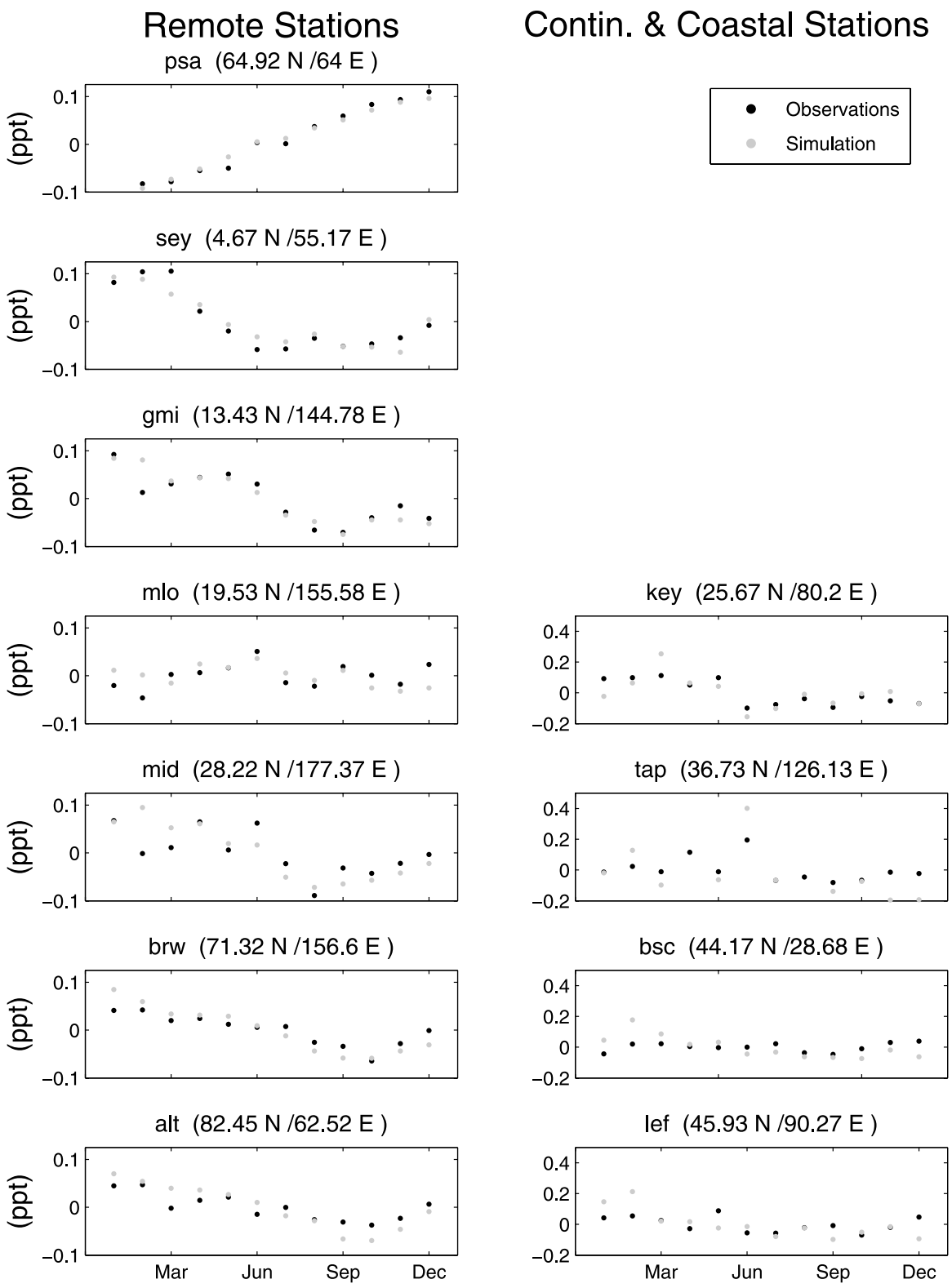

Figure 3. Detrended observed and simulated monthly mean records for the year 1998 (for details see main text).

3.1.3. Continuous Records: Near-Surface Air Parcel Paths, High SF_6 Events, and PBL Ventilation

[25] Quasi-continuous records resolve the time spectrum of SF_6 variations caused by the interplay of advection and mixing acting on the pointlike SF_6 emissions. Information on the accuracy of predicted advection and the relative importance of advective and diffusive processes is contained in the amplitude, frequency and phase of SF_6 variations.

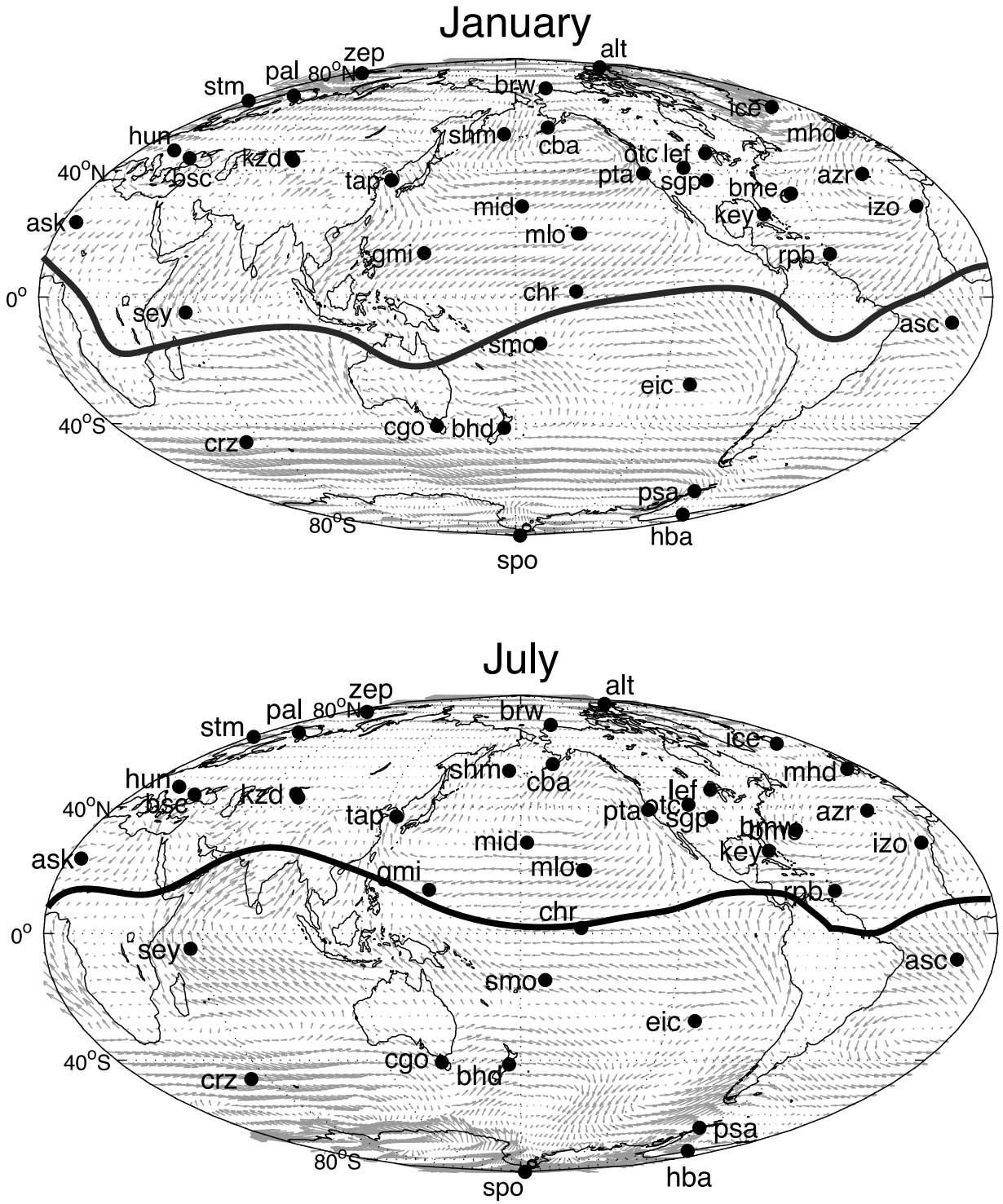

Figure 4. Monthly mean surface winds for 1995, surface site location and Intertropical Convergence Zone (ITCZ).

[26] Depending on the site location relative to emissions, the nature of quasi-continuous data varies considerably. Quasi-continuous data from the 396 m level of the Wisconsin tall tower (LEF, 45.93°N, 90.27°W) (Figure 5) [*Hurst et al.*, 1998] exhibit a very well defined background line on which pollution events are "superposed." Signals are on the order of 1.5 ppt which is large (for comparison the inter-hemispheric difference is ~0.36 ppt). For the interpretation of the other three records (Figure 6) it is important to know that the data records are filtered while the simulated records are not. We have filtered the data because they exhibit high frequency variability caused by mesoscale or shorter-scale events not simulated by the model, or by short-term imprecision in the measurement system. For the filtering

Table 3. Data-Model Comparison Summary of Seasonal Cycles at Surface Sites, 1998–2000

Site	Seasonal Amplitude, ppt	$Std(X^{obs} - X^{sim})$, ppt	Time Correlation r (−)	$Std(X^{obs})$, ppt	$Std(X^{sim})$, ppt
		Continental and Coastal Sites			
KEY	0.15	0.06	0.86	0.04	0.07
TAP	0.15	0.19	0.72	0.05	0.09
BSC	0.1	0.07	0.26	0.03	0.02
LEF	0.1	0.09	0.42	0.03	0.05
		Remote Oceanic Sites			
PSA	0.1	0.01	0.40	0.02	0.01
SEY	0.17	0.02	0.94	0.01	0.01
GMI	0.05	0.02	0.93	0.02	0.01
MLO	0	0.02	0.47	0.02	0.01
MID	0.05	0.04	0.72	0.02	0.01
BRW	0.05	0.02	0.64	0.01	0.01
ALT	0.05	0.03	0.60	0.01	0.01

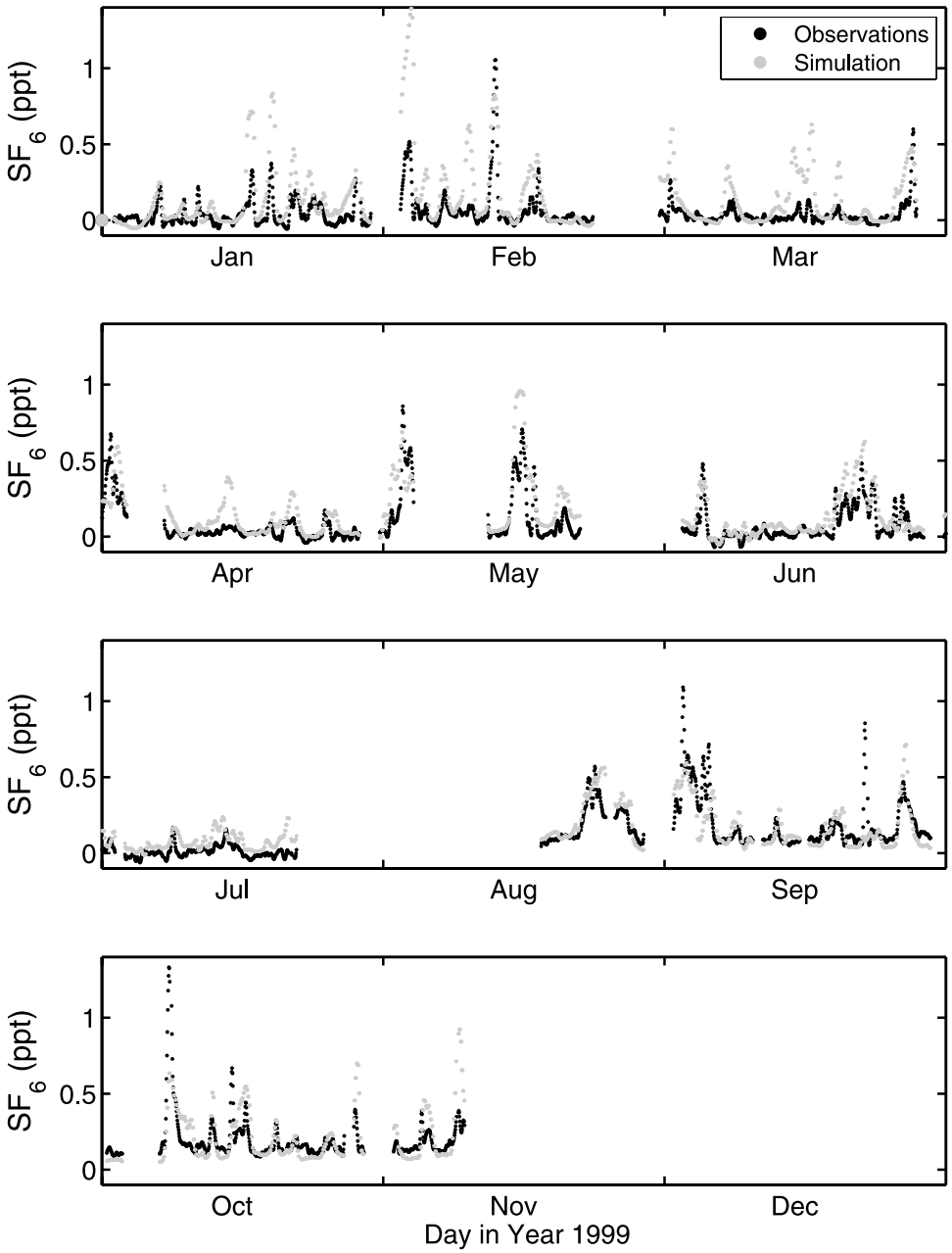

Figure 5. Observed and simulated SF_6 record at 396 m above ground at the Wisconsin tall tower (LEF), 45.93°N, 90.27°W (annual means subtracted).

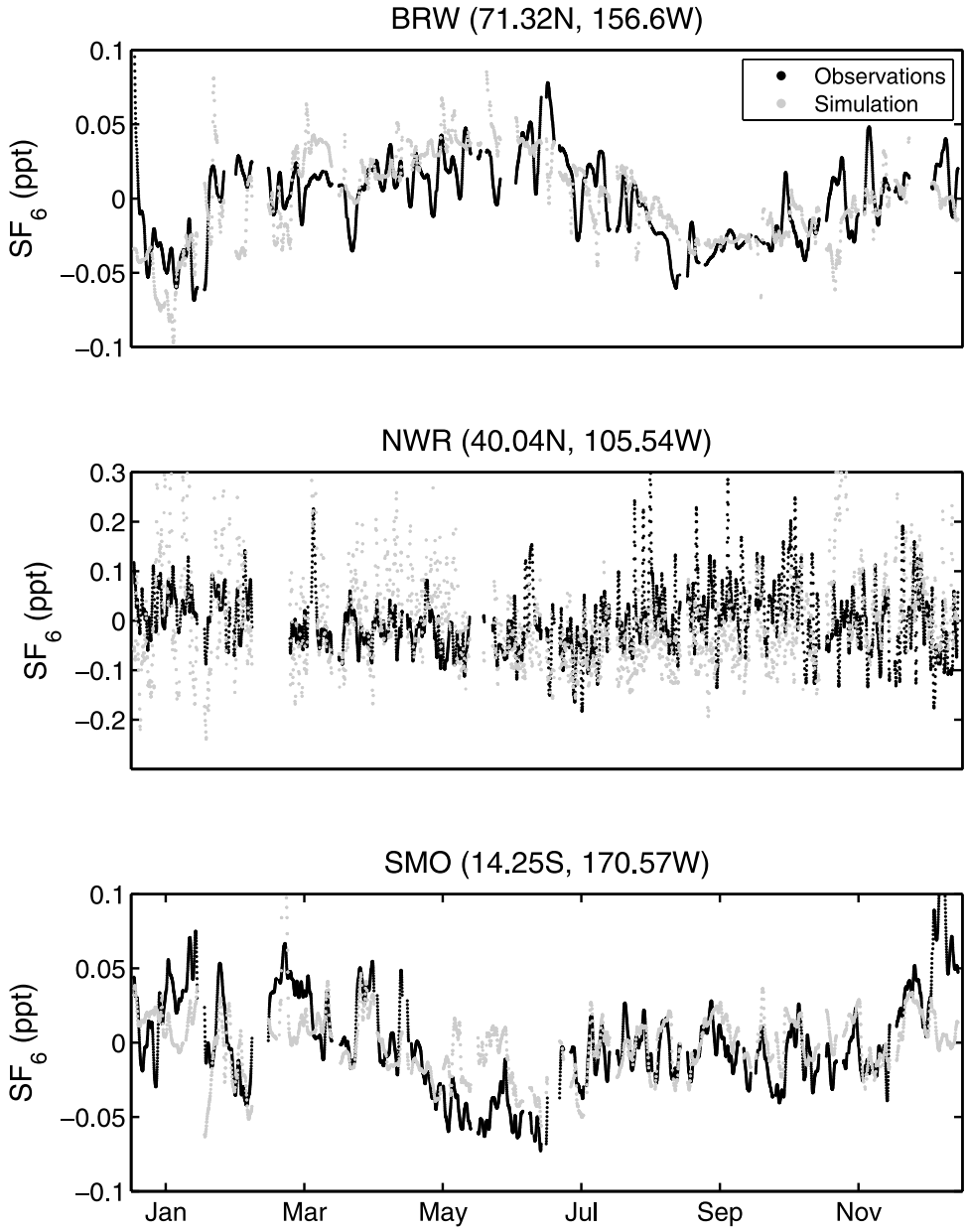

Figure 6. Observed and simulated SF_6 records at Barrow (71.32°N, 156.6°E), Niwot Ridge (40.04°N, 105.54°W), and Samoa (14.25°S, 170.57°W) during 2001.

we used a cutoff frequency of 1/2 d^{-1}. For display, we also removed a linear trend from both observations and simulations to expose clearly the temporal variability (Figures 5 and 6).

[27] In contrast to the Wisconsin record, no clear baseline can be identified at Pt. Barrow, Alaska (BRW, 71.32°N, 156.6°W) and American Samoa (SMO, 14.25°S, 170.57°W), and the amplitude of synoptic variations is considerably smaller. Variation of signals at Samoa and Barrow are on the order of 0.1 ppt and at Niwot Ridge, Colorado (NWR, 40.04°N, 105.54°W) on the order of 0.3 ppt. Compared to the Samoa and Barrow records, the Niwot Ridge continuous record exhibits higher frequency variations, due in part to changing wind conditions that bring polluted air west (upslope) from the Boulder/Denver metro area and clean air east (downslope) from the mountains (T. Thompson, personal communication, 2006).

[28] Comparison with simulations shows that they reproduce observed high-SF_6 events at LEF very well. Within the one year period displayed, only two, or ≈5%, of predicted events are either absent in the observation record or only very weakly discernable. As the flushing timescale of the PBL was previously estimated to be ≈1.5 days [e.g., *Gloor et al.*, 2001] this indicates that advective transport on a timescale of ≈1.5 days is very well represented by the model, that the spatial patterns of surface fluxes used for the simulations are quite realistic, and that the quality of the LEF data is excellent. The comparison also reveals that during winter the model simulations overestimate the PBL-free troposphere difference (the difference between events and the base line) by approximately a factor 2; that is,

PBL ventilation during winter is likely too weak in the model.

[29] Model-data agreement at the other three sites is worse. While the model seems to capture phasing of short-term variation at Niwot Ridge (NWR), the amplitude of the variations is overestimated approximately threefold during November to April and underestimated during summer by a similar factor. At Barrow the main seasonal cycle is captured and there is sporadic agreement in phasing of events. The Barrow record is particularly variable, therefore we do not draw quantitative conclusions. Finally, because of the large distance of Samoa from significant emissions (distance $\approx$ 1000 km), the Samoa record is a good test for the models predictive capability of advection on timescales on the order of a week. The amplitude of variations is approximately 30 fold smaller compared to the Wisconsin record. Magnitude and phasing of variation agrees well particularly for the second half of the year.

[30] With concerns on data quality in some instances, the data simulation comparison indicates that advective transport on timescales up to $\approx$1 week is quite successful. Without these concerns, time-power-spectral analysis of the quasi-continuous records at BRW, SMO and NWR, would provide more quantitative information. The comparisons finally reveal that the quasi continuous tall tower record at Wisconsin (LEF), which samples both polluted and unpolluted air sectors, provides a strong constraint on the realism of PBL ventilation in models.

3.1.4. PBL-Free Troposphere Differences

[31] Vertical SF_6 profiles contain information about PBL ventilation as well as on the pathways of Northern Hemisphere midlatitude emissions throughout the entire troposphere, including the upper tropical troposphere. To illustrate this information we present NOAA ESRL aircraft records from the six sites that extend the farthest back in time and that sample a representative range of observed signals (Figure 7). Signals include the E-W differences in surface emission strength across the USA (Poker Flats Alaska (PFA) 65.07°N, 147.29°W, LEF, 45.93°N, 90.27°W, CAR, Carr, Colorado, 40.90°N, 104.8°W, Harvard Forest, Massachusetts (HFM) 42.54°N, 72.17°S), and the vertical SF_6 distribution at Northern Hemisphere remote locations (PFA) versus the tropics and the Southern Hemisphere (Fortaleza, Brazil (FTL) 4.15°S, 38.28°W, Rarotonga, Cook Islands (RTA) 21.25°S, 159.83°W).

[32] Vertical profiles across the US reveal the following. At Harvard Forest (HFM), which is located near a strong emission region, there is a clear two-layer structure with a near-surface layer of $\approx$2 km height and a "free troposphere" layer above it. The difference between the two layers is that mixing ratios decrease at a different rate with height. No clear layered structure is observed in the other North American profiles. This is not due to the averaging of profiles over time as each individual profile (Figure 7) is obtained over a few hours. Profiles from the other USA sites (PFA, CAR and LEF) do not show this two-layer structure, presumably because they are more distant from strong surface emissions than HFM. None of these profiles reveal a well-mixed surface layer, in contrast to atmospheric properties (e.g., potential temperature). Generally, the USA profiles show a negative vertical gradient in SF_6 mixing ratio (i.e., decreasing with altitude), with some evidence of polluted layers aloft.

[33] Proximity of the observations to surface emissions is reflected both in magnitude and intermittence in the PBL-free troposphere difference. The closer the sites are to large surface emissions, the larger the difference in signal and variance (Table 4). The HFM (42.54°N, 72.17°S) signal provides a rough estimate of the annual mean PBL-free troposphere gradient signal per local flux strength, which is 0.17 ppt/1.28×10^{-7} moles m^{-2} s^{-1}. The flux strength is the $1° \times 1°$ value from the *Olivier* [2002] flux compilation corresponding to the HFM location.

[34] Generally during summer the PBL-free troposphere difference is reduced compared to winter. Other than due to seasonality and with exception of occasional high-SF_6 events, the vertical shape of the profiles changes only slightly. Examples of high SF_6 events at CAR and LEF in May 2003 are indicated in Figure 7 with arrows.

[35] Finally, vertical gradients of tropical and Southern Hemisphere profiles (FTL, 4.15°S, 38.28°W, and RTA, 21.25°S, 159.83°W) differ from the Northern Hemisphere profiles in sign, indicating that in the Southern Hemisphere signals propagate from the upper troposphere to the lower troposphere.

[36] Simulations reproduce spatial and temporal variation of the observations qualitatively fairly well. The vertical shape of the profile including the contrast between North America sites versus tropical and Southern Hemisphere sites is captured. Generally, observed profiles are less smooth in the vertical compared to simulation predictions, as is expected from the mismatch in scale of a model grid cell versus air volume sampled. The time course characterized by a stronger increase at Northern Hemisphere sites during winter compared to summer agrees well. Finer features, like the jump in SF_6 between February and March at RTA and the reversal of the vertical gradient in December at the same site, are reproduced as well.

[37] Quantitative characteristics of PBL (0–2 km) free troposphere (3–6 km) differences and their modeling are summarized in Table 4. Prediction of the difference has both large variance and is biased. The bias exposes primarily deficiencies in predicting the PBL concentration and not so much the free troposphere concentration (as the observed free troposphere concentrations across Northern Hemisphere midlatitudes are fairly uniform). When combining the data from Northern Hemisphere sites, the model's overprediction of PBL SF_6 by a factor 2 over North America during winter is statistically significant. There are two possible causes of the overestimation of PBL SF_6: (1) the spatial distribution and magnitude of SF_6 fluxes is incorrect and (2) PBL ventilation over continents is not correctly modeled. The quasi-continuous record at LEF discussed above indicates that the spatial distribution over North America is likely accurate. The excellent agreement at Northern Hemisphere remote sites including Mace Head, Ireland (MHD) 53.33°N, 9.9°W, Azores, Portugal (AZR) 38.77°N, 27.38°W, Kazakhstan (KZD) 44.45°N, 75.57°W, Shemya, Alaska (SHM) 52.72°N, 174.1°E, Cold Bay, Alaska (CBA) 55.20°N, 162.72°W, and of the interhemispheric difference both near the surface and in the upper troposphere (see below) indicates furthermore that the flux strength is fairly accurate as well. Together this indicates

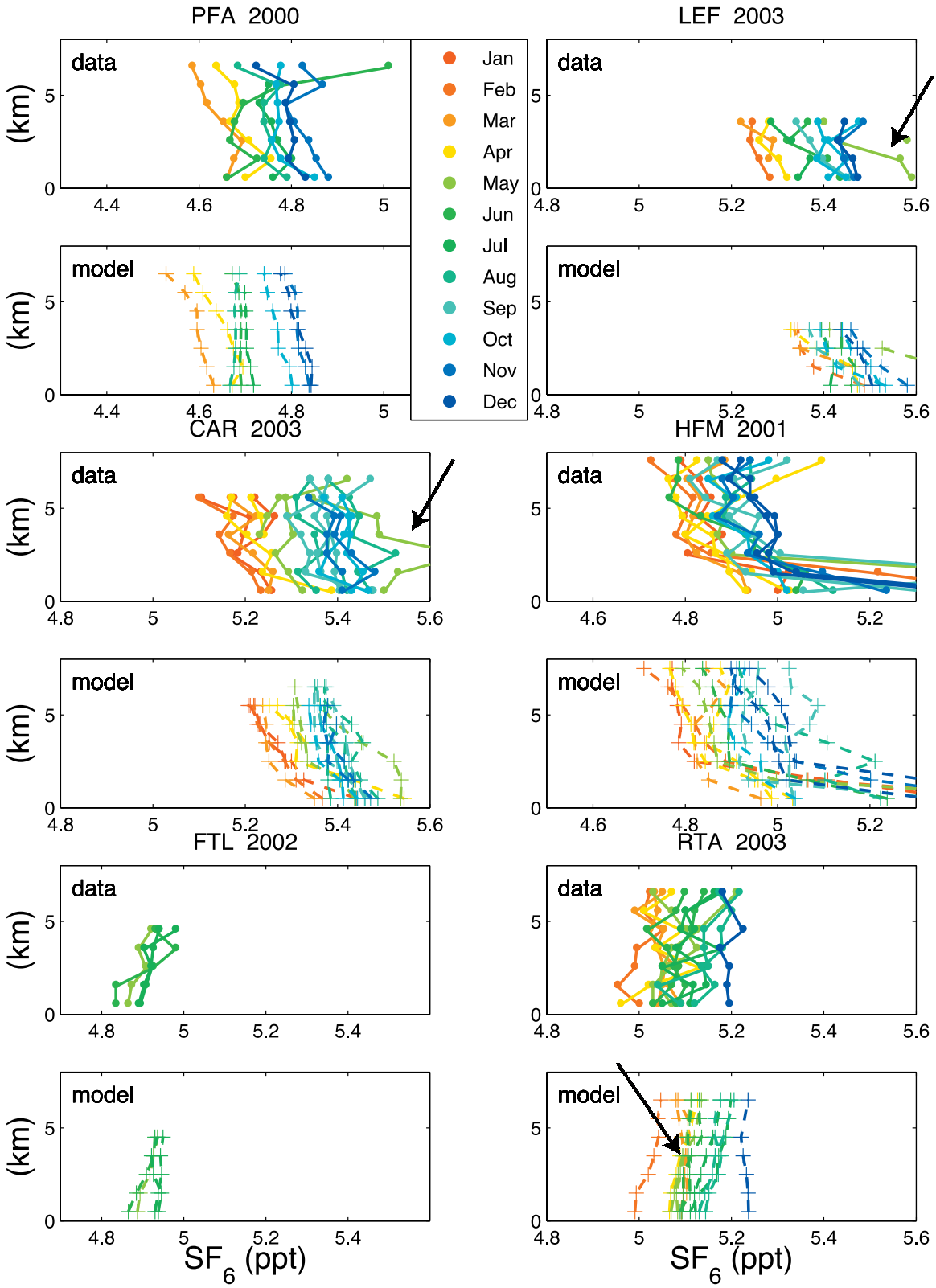

Figure 7. Individual observed (top plot for each site) and simulated (bottom plot for each site) vertical SF_6 profiles for selected years. Arrows indicate high SF_6 events. The shading indicates the month during which the profiles have been measured. The profile data are averaged over 50 m vertical bins.

Table 4. Data-Model Comparison Summary of PBL Free Troposphere Difference $\Delta X \equiv \overline{X}^{0-2km} - \overline{X}^{3-6km}$, Where the Overbar Refers to an Average Over the Period From 1998 to 2003[a]

Site	ΔX^{obs}, ppt	ΔX^{sim}, ppt	$Std(\Delta X^{obs})$, ppt	$Std(\Delta X^{sim})$, ppt	$Std(\Delta X^{obs} - \Delta X^{sim})$, ppt	Time Correlation (−)	SF_6 Emiss, mol m^{-2} s^{-1}
PFA	0.01	0.02	0.03	0.02	0.02	0.63	0
LEF	0.05	0.11	0.06	0.1	0.08	0.64	1.3×10^{-8}
CAR	0.04	0.09	0.05	0.06	0.06	0.43	2.43×10^{-9}
HFM	0.22	0.23	0.15	0.2	0.22	0.26	1.3×10^{-7}
FTL	−0.06	−0.03	0.04	0.02	0.04	0.28	7.6×10^{-11}
RTA	−0.03	−0.02	0.03	0.02	0.03	0.43	0

[a]Time correlation refers to the correlation coefficient between the time series of observed and simulated PBL-free troposphere differences over the period 1998 to 2003 and similar for standard deviation (Std). Sites remote from emission are not italicized.

strongly that biases reflect model deficiencies rather than SF_6 flux biases.

[38] The time correlation of the PBL-free troposphere differences over the period from March 2000 to December 2003 is fairly high with exception of HFM, which is located very close to large emissions. The high correlation is an indicator that signals are zonally well propagated by the model.

[39] The main constraint provided by vertical aircraft profiles in addition to surface values is the PBL free troposphere contrast. Observed differences between SF_6 mixing ratios in the PBL and free troposphere can be as great as 1 ppt, roughly three times the interhemispheric gradient. Signal and standard deviation of this constraint are summarized in Table 4. Independent of the site's location, the ratio of the mean vertical difference to the standard deviation of the vertical difference is close to unity; i.e., the constraint provided by a single profile is weak, likely as a reflection of the mismatch between model resolution and processes that ventilate the PBL. However, taking advantage of the observation that profile shapes do not vary that much during a season, counting statistics may be used to estimate a seasonal mean PBL-free troposphere difference (i.e., a winter and a summer mean difference) to increase this ratio by approximately a factor 4, which results in a substantially more favorable "signal to noise" ratio of the constraint on PBL-free troposphere ventilation in models.

3.2. Upper Troposphere Signals: Interhemispheric Gradient and Temporal Variability

[40] Upper air transects contain information about the relation between surface and upper troposphere signals and the transport mechanisms involved.

[41] The aircraft upper troposphere transect that was measured most frequently amongst all CARIBIC aircraft tracks runs between Germany and Sri Lanka. The records in Figure 8 reveal (1) largest variation at the 40–50°N latitudinal band which corresponds to the level with lowest potential temperature (see companion paper) and (2) a N-S latitudinal mean difference between 40–50°N and 10–20°N of 0.04 ppt (standard deviation 0.07 ppt) (compared to 0.2 ppt in near surface records (standard deviation 0.05 ppt)).

[42] The Germany-Africa transect reaches the farthest south amongst all airplane tracks and therefore is best suited to investigate the upper troposphere N-S gradient (Figure 9) and its relation to the surface gradient. The upper troposphere N-S gradient at ≈10 km height is again substantially smaller compared to the surface gradient (slope reduced by factor 2.5 (upper troposphere difference = 0.15 ppt, surface difference = 0.38 ppt)). Furthermore it is noteworthy (1) that the 10 km altitude concentrations seem to intersect the surface concentration level in the tropics with higher concentrations in the Southern Hemisphere at 10 km height compared to the surface and (2) that the latitudinal gradient is more uniform aloft than near the surface.

[43] Vertical aircraft profiles permit us also to look into the relation between Northern Hemisphere and Southern Hemisphere signals, both at the surface and in the mid-to-upper troposphere. The two sites that span the largest latitude difference and the longest records of vertical profiles are Poker Flat, Alaska (PFA) and Rarotonga (RTA) (Figure 10). Measurements from these sites seem to indicate some correlation between upper troposphere records at PFA and RTA but no correlation with near surface SF_6 at RTA, which potentially holds clues about north-south transport via the upper troposphere (to be discussed in a companion paper).

[44] Comparison of the observational records with model predictions (Figure 8) reveal generally excellent data-simulation agreement both in magnitude and time variations (summarized in Table 5). There is some underestimation of the amplitude of the variability in the 40–50°N latitude band

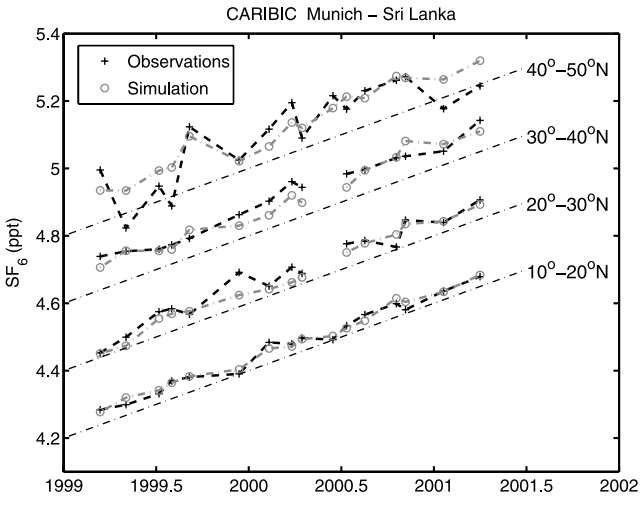

Figure 8. Average over 10° latitude bands of upper troposphere SF_6 measured on aircraft traveling at approximately 10 km height between Munich (Germany) and Sri Lanka. The data north from 20°N are successively offset by 0.2 ppt. The dash-dotted lines are offset by 0.2 ppt to provide a reference.

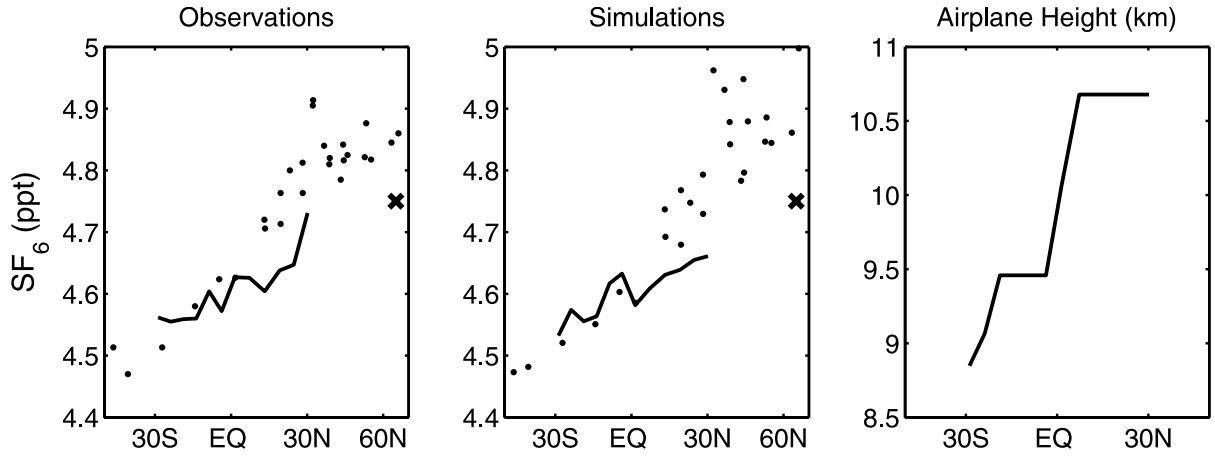

Figure 9. Observed surface site (dots) and upper troposphere SF_6 (bold line and cross). Surface data are from the NOAA ESRL network, upper troposphere data from a flight from Germany to Cape Town (South Africa) and from the top kilometer of vertical profiles at Poker Flats, Alaska (crosses, mean of October 2000 and April 2001 data).

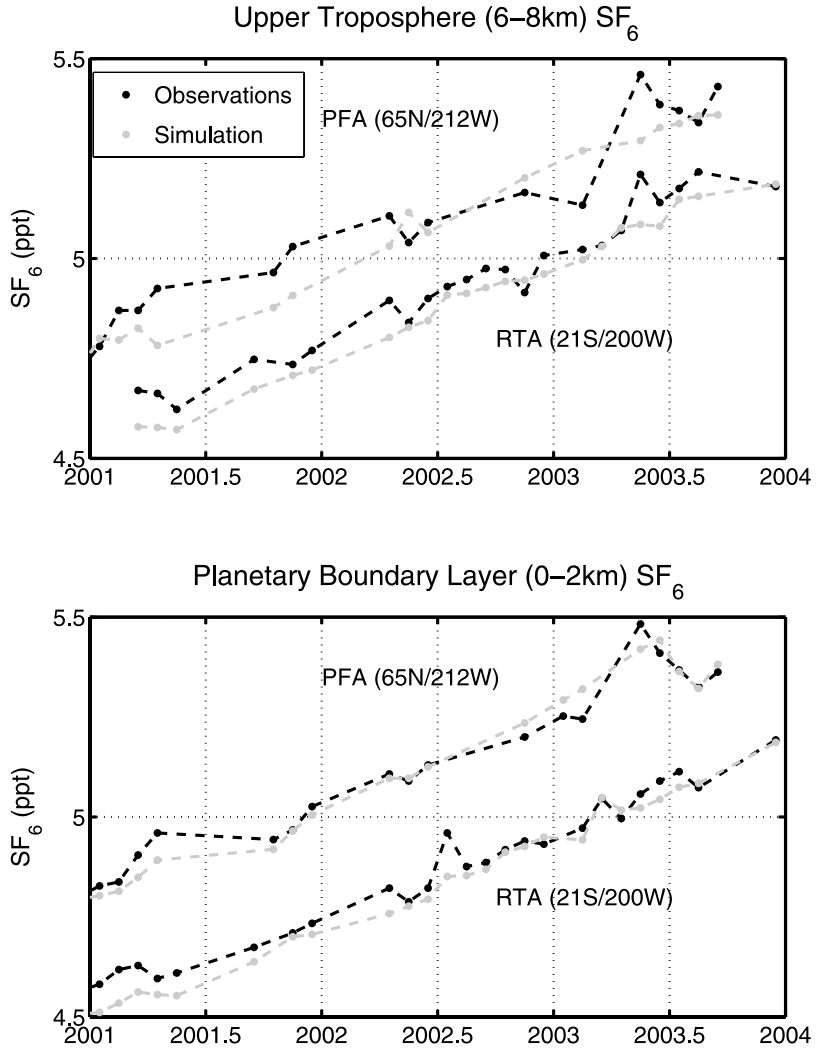

Figure 10. Modeled and observed SF_6 at Poker Flats, Alaska and Rarotonga averaged for 0 to 2 km and 6 to 8 km height above ground, respectively.

Table 5. Data-Model Comparison Summary of Upper Troposphere Aircraft Transects From Germany to Sri Lanka, 1999–2002

Latitude Range	Bias	Time Correlation	Std (Detrended Signal)
10–20°N	−0.01	0.91	0.03
20–30°N	0.01	0.98	0.03
30–40°N	0.01	0.98	0.02
40–50°N	0.00	0.99	0.07

indicating possibly not sufficiently efficient transport from the surface. Modeled N-S differences in the upper troposphere agree also well with observations. Altogether this suggests that transport pathways of Northern Hemisphere midlatitude surface emissions via the upper troposphere predicted by the model is consistent with the observations.

4. Summary, Implications, and Conclusions

[45] The purpose of this first of two companion papers is to identify and characterize partially known observational constraints from a range of SF_6 data, and to use them to determine accuracy (uncertainty and biases) of transport predictions with the MOZART-2 atmospheric chemistry and transport model. Main noteworthy observational findings are (1) a well known steep N-S gradient at the surface confined to an ≈40° wide latitude band in the tropics; (2) a fairly uniform N-S gradient in the upper troposphere (at ≈10 km); (3) a weak time correlation between Northern Hemisphere high-altitude and Southern Hemisphere high-altitude records, but not with Southern Hemisphere surface records; (4) a negative concentration gradient in vertical profiles measured from the surface to 8 km altitude in the Northern Hemisphere, but positive gradient in the Southern Hemisphere; (5) an increase in the temporal variation in upper troposphere Northern Hemisphere records with increasing latitude; and (6) a clear reflection in surface records of large-scale seasonal movements and changes of the atmospheric state like the undulations of the Intertropical Convergence Zone (ITCZ) and the Arctic winter circulation. The strength of these constraints as characterized by the ratio of the mean signal and its standard deviation is largest for the interhemispheric difference (ratio ∼10), followed by seasonal cycles in the tropics and high northern latitudes (∼8), PBL-free troposphere difference from vertical profiles when seasonally averaged (ratio ∼4), and upper troposphere latitudinal gradient (∼4) (Table 6).

[46] With regards to transport modeling accuracy of the MOZART-2 model, SF_6 data simulation comparisons reveal (1) accurate reproduction of the surface interhemispheric difference based on surface remote sites (systematic bias ≤ 5%); (2) small variance in model-observation differences over the course of a year at remote surface sites and the upper troposphere (≤ 5% of the surface interhemispheric difference); (3) good model reproduction of the phasing of high SF_6 events (≤ 5% of events missed both at a continental site like the Wisconsin tall tower (USA) and more remote sites like Samoa), indicating faithfulness of advection on timescales up to ≈1 week, which is consistent with the results of *Peters et al.* [2004] who analyzed transport simulated with the TM5 transport model; (4) that the shape of vertical profiles is well captured but the magnitude of lower to free troposphere differences is often overestimated in the model over Northern Hemisphere continents during winter, and the data exhibit larger variance over the column, both findings also consistent with the *Peters et al.* [2004] study; (5) a general underestimation of near surface to free troposphere difference during winter at the Wisconsin (LEF) continental site; (6) that large-scale seasonal movements of the troposphere like undulation of ITCZ and Arctic winter circulation clearly seen in the data are very well captured by the simulations (accuracy ∼ 0.02 ppt given a signal of 0.17 ppt at SEY); and (7) that upper troposphere N-S differences and temporal variation are well captured as well. The data-simulation comparisons also permit an estimate of representation errors due to energy-related emissions, which is relevant for estimating CO_2 sources and sinks using inverse modeling. Representation errors due to this error source when translated to CO_2 is ∼1 ppm for continental sites like LEF and ∼2.5 ppm for sites located in continental

Table 6. Summary of Observed Signals, Model-Data Agreement, and "Signal to Noise" Ratio of Constraint Provided by the Signal

Diagnostic	Signal, ppt	Sensitivity to Flux	Bias, ppt	Corr (−)	STD_{obs}, ppt	SNR (−)
Remote surface sites						
Annual mean interhemispheric difference	0.36	0.07[a]	6.5%	0.99	0.05	10
Annual mean RMS	0.03					
Seasonal signal	≤0.2			∼0.8	0.02	≤10
Coastal surface sites						
Representation error TAP, KEY	0.2					
Continental vertical profiles						
PBL-free troposphere difference	0.05–0.2	1.3*10[6b]	up to 100%	0.03–0.15	0.03–0.22	1 (profile), 4 (season)
Continental continuous records						
Magnitude – events at LEF (PBL-free troposphere difference)	1.5		up to 100%	0.8		5–10
Synoptic advective transport	1.5			≥0.9		10
Upper air transects: Interhemispheric difference						
Germany – Cape Town	0.15					∼5
Germany – Cape Town, surface	0.38					
Germany – Sri Lanka	0.04		∼0.01	0.98		
Germany – Sri Lanka, surface	0.2					
Remote continuous records						
Advective transport						

[a]Unit of interhemispheric difference sensitivity to emissions is ppt (kt $yr^{-1})^{-1}$).
[b]Unit for PBL-free troposphere difference sensitivity to emissions at Harvard forest (HFM) is moles m^{-2} s^{-1}.

Table A1. Name, Abbreviation, and Location of Observation Sites From Which Records Are Displayed

Site Name	Abbreviation	Latitude	Longitude	Altitude, m asl
Alert	ALT	82.45°N	62.52°W	210
Barrow	BRW	71.32°N	156.6°W	11
Black Sea, Constanta	BSC	44.17°N	28.68°E	3
Carr	CAR	40.90°N	104.8°W	N/A, profile
Guam	GMI	13.43°N	144.78°E	6
Harvard Forest	HFM	42.54°N	72.17°S	N/A, profile
Key Biscayne	KEY	25.67°N	80.2°W	3
Fortaleza	FTL	4.15°S	38.28°W	N/A, profile
Mauna Loa	MLO	19.53°N	155.58°W	3397
Midway	MID	28.22°N	177.37°W	7.7
Niwot Ridge	NWR	40.04°N	105.54°W	3013
Park Falls	LEF	45.93°N	90.27°W	470
Rarotonga	RTA	21.25°S	159.83°W	N/A, profile
Seychelles	SEY	4.67°S	55.17°E	7
Samoa	SMO	14.25°S	170.57°W	77
Taeahn Peninsula	TAP	36.73°N	126.13°E	20

outflow regions like TAP (36.73°N, 126.13°E) and KEY (25.67°N, 80.2°W).

[47] In terms of transport processes the model thus reproduces well (1) interhemispheric transport, (2) advection of individual air parcels on timescales of hours to weeks, and (3) pathways of Northern Hemisphere midlatitude surface emissions through the upper troposphere to the Southern Hemisphere. It reproduces less well PBL-free troposphere exchange over the continents particularly during winter. Items 1 and 3 taken together indicate that PBL-free troposphere exchange over continents is not a crucial (limiting) step to reproduce large-scale transport features at remote oceanic locations and the upper troposphere. This is similar to the finding in ocean models that anthropogenic CO_2 uptake by the oceans is largely insensitive to parameterization of air-sea gas exchange because it is not the limiting transport step [*Sarmiento et al.*, 1992] (the limiting step is transport from the mixed layer to deeper parts of the ocean).

[48] What are the implications on existing inverse modeling results for CO_2? For inverse calculations based on remote sites the uncertainty of flux estimates due to imperfections of transport alone is on the order of 10% (which is 0.6 PgC yr^{-1} for Northern Hemisphere midlatitude carbon fluxes around the year 2000 for fossil fuel emissions alone). Use of Northern Hemisphere continental winter time data will tend to bias flux estimates for the winter toward half the correct magnitude when based on the MOZART-2 model (because the model overestimates twofold the PBL signal per flux strength). In contrast much smaller biases are expected when only remote oceanic stations are used in these calculations. Finally ''representation'' errors are particularly large at coastal ocean sites located in continental outflow regions and therefore need to be assigned appropriately large uncertainties.

[49] What recipe follows from the results for assigning uncertainties caused by modeling imperfection to data used in inverse calculations of atmospheric transport to estimate surface fluxes? Provided that modeling uncertainties can be translated into equivalent data uncertainties, observations at remote sites should be assigned an uncertainty due to modeling alone of 10% of the interhemispheric difference resulting from a Northern Hemisphere flux located in the Northern Hemisphere typical for the problem at hand. For vertical profile data on continents a bias of ~100% should be assumed during wintertime and an uncertainty of 100% of typical signal magnitude. Uncertainties of upper troposphere data should be assigned an uncertainty on the order of 25%.

[50] Finally the results of this study suggest that the uncertainties in SF_6 flux estimates based on sales numbers and energy use, scaled with the global mean atmospheric SF_6 record, lead to very good agreement between model predictions and data. In our view therefore SF_6 remains currently the most quantitative and therefore most valuable constraint on tropospheric transport and its modeling.

Appendix A

[51] Specifics of sites where SF_6 atmospheric concentration data that are analyzed in this paper have been measured are provided in Table A1.

[52] **Acknowledgment.** Manuel Gloor acknowledges support from NOAA award NA17RJ2612.

References

Denning, A. S., et al. (1999), Three-dimensional transport and concentration of SF_6: A model intercomparison study (Trnascom2), *Tellus, Ser. B*, *51*, 266–297.

Geller, L. S., J. W. Elkins, J. M. Lobert, A. D. Clarke, D. F. Hurst, J. F. Butler, and R. C. Myers (1997), Tropospheric SF_6: Observed latitudinal distribution and trends, derived emissions and interhemispheric exchange time, *Geoophys. Res. Lett.*, *24*, 675–678.

Gloor, M., S.-M. Fan, J. Sarmiento, and S. Pacala (2000), Optimal sampling of the atmosphere for purpose of inverse modeling: A model study, *Global Biogeochem. Cycles*, *14*, 407–428.

Gloor, M., P. Bakwin, D. Hurst, L. Lock, R. Draxler, and P. Tans (2001), What's the concentration footprint of a tall tower?, *J. Geophys. Res.*, *106*, 17,831–17,840.

Hack, J. J. (1994), Parameterization of moist convection in the NCAR community climate model (CCM2), *J. Geophys. Res.*, *99*, 5551–5568.

Holtslag, A., and B. Boville (1993), Local versus nonlocal boundary-layer diffusion in a global climate model, *J. Clim.*, *6*, 1825–1842.

Horowitz, L. W., et al. (2003), A global simulation of tropospheric ozone and related tracers: Description and evaluation of MOZART, version2, *J. Geophys. Res.*, *108*(D24), 4784, doi:10.1029/2002JD002853.

Hurst, D. F., P. S. Bakwin, and J. W. Elkins (1998), Recent trends in the variability of halogenated trace gases over the United States, *J. Geophys. Res.*, *103*(D19), 25,299–25,306.

Kjellstrom, E., J. Feichter, and G. Hoffmann (2000), Transport of SF_6 and $^{14}CO_2$ in the atmospheric general circulation model ECHAM4, *Tellus, Ser. B*, *52*, 1–18.

Ko, M. K. W., N. D. Sze, W. Wang, G. Shia, A. Goldman, F. J. Murcray, D. G. Murray, and C. P. Rinsland (1993), Atmospheric sulfur hexafluoride: Sources, sinks and greenhouse warming, *J. Geophys. Res.*, *98*, 10,499–10,507.

Lin, S.-J., and R. Rood (1996), Multidimensional flux-form semi-Lagrangian transport schemes, *Mon. Weather Rev.*, *124*, 2046–2070.

Lloyd, J., et al. (2002), A trace-gas climatology above Zotino, central Siberia, *Tellus B*, *54*(5), 749–767, doi:10.1034/j.1600-0889.2002.01335.x.

Maiss, M., and I. Levin (1994), Global increase of SF_6 observed in the atmosphere, *Geophys. Res. Lett.*, *21*(7), 569–572.

Maiss, M., L. P. Steele, R. J. Francey, P. J. Fraser, R. L. Langenfelds, N. B. A. Trivett, and I. Levin (1996), Sulfur hexafluoride—A powerful new atmospheric tracer, *Atmos. Environ.*, *30*, 1621–1629.

Olivier, J. G. J., (2002), Part III: Greenhouse gas emissions: 1. Shares and trends in greenhouse gas emissions; 2. Sources and Methods; Greenhouse gas emissions for 1990 and 1995, in *CO2 Emissions From Fuel Combustion 1971–2000*, pp. III.1–III.31, Int. Energy Agency, Paris.

Peters, W., M. C. Krol, P. Begamaschi, G. Dutton, P. van Velthoven, J. B. Miller, L. Bruhwiler, and P. P. Tans (2004), Toward regional-scale modeling using the two-way nested global model TM5: Characterization of transport using SF_6, *J. Geophys. Res.*, *109*, D19314, doi:10.1029/2004JD005020.

Ravishankara, A. R., S. Solomon, A. A. Turnispeed, and R. F. Warren (1993), Atmospheric lifetime of long-lived halogenated species, *Science*, *259*, 194–199.

Sarmiento, J. L., J. C. Orr, and U. Siegenthaler (1992), A perturbation simulation of CO_2 uptake in an ocean general circulation model, *J. Geophys. Res.*, *97*(C3), 3621–3645.

Simmons, A. J., and J. K. Gibson (2000), The ERA-40 project plan, *ERA-40 Proj. Rep. Ser. 1*, Eur. Cent. for Med.-Range Weather Forecasts, Reading, U. K.

Zhang, G. J., and N. A. McFarlane (1995), Sensitivity of climate simulations to the parameterization of cumulus convection in the Canadian Climate Cntre general circulation model, *Atmos. Ocean*, *33*, 407–466.

C. Brenninkmeijer, Air Chemistry Department, Max-Planck Institute for Chemistry, P.O. Box 3060, D-55020 Mainz, Germany.

C. Crevoisier, Atmospheric and Oceanic Sciences Program, Princeton University, Sayre Hall, Forrestal Campus, Princeton, NJ 08540, USA.

E. Dlugokencky, G. Dutton, D. F. Hurst, and P. Tans, Global Monitoring Division, Earth System Research Laboratory, NOAA, 325 Broadway R/GMD1, Boulder, CO 80305-3328, USA.

M. Gloor, Earth and Biosphere Institute, School of Geography, University of Leeds, Woodhouse Lane, Leeds LS2 9JT, UK. (e.gloor@leeds.ac.uk)

L. Horowitz, Geophysical Fluid Dynamics Laboratory, NOAA, Forrestal Campus, 201, Forrestal Road, Princeton, NJ 08540, USA.

T. Machida, Atmospheric Measurement Section, National Institute for Environmental Studies, 16-2 Onagawa, Tsukuba 305-0053, Japan.